ADVANCEMENTS IN UNDERSTANDING THE 2-D ROLE OF IMPURITY RADIATION FOR DISSIPATIVE DIVERTOR OPERATION ON DIII-D

C.M. SAMUELL, A.G. MCLEAN, S.L. ALLEN, M.E. FENSTERMACHER, C.J. LASNIER, G.D. PORTER, T.D. ROGNLIEN, F. SCOTTI, V. SOUKHANOVSKII, W.H. MEYER
Lawrence Livermore National Laboratory
Livermore, California, USA
Email: mclean@fusion.gat.com

A.E. JAERVINEN, A. HOLM, M. GROTH
Aalto University
Espoo, Finland

D.A. ENNIS, C.A. JOHNSON
Auburn University
Auburn, Alabama, USA

F. GLASS, H. GUO, A.W. LEONARD, A.L. MOSER, D. THOMAS, H.Q. WANG
General Atomics
San Diego, California, USA

J.D. WATKINS
Sandia National Laboratory
Albuquerque, New Mexico, USA

J. BOEDO, E.M. HOLLMANN
University of California San Diego
San Diego, California, USA

R.S. WILCOX
Oak Ridge National Laboratory
Oak Ridge, Tennessee, USA

Abstract

Recent analysis leveraging the broad array of measurable plasma parameters on the DIII-D tokamak has been used to elucidate the physics processes underlying detachment processes in the divertor and reveal the 2D nature of detachment important for design of detachment scenarios for next stage devices. The dominant role of EUV/VUV radiation for radiative power exhaust has been established experimentally with accompanying spectroscopy leveraged alongside collisional radiative modelling to calculate the impurity density, its concentration in the plasma, and the charge-state distribution in the divertor. These measurements, the use of reduced models for rapid interpretation, and their comparison to boundary modelling are critically essential for validation of recent scalings for the impurity concentration required for detachment in future fusion devices. In this work, coincident 2-D measurement of critical plasma parameters for power exhaust studies (n_e, T_e, P_{rad}, $E_{VUV/EUV}$) reveal the physics of dissipation mechanisms, non-Coronal effects, target asymmetries, charge exchange and transport involved in the divertor dissipation process and show qualitative agreement with recent detachment scalings. Specifically, direct quantitative comparison to modelling demonstrates a greater radial emission extent compared to UEDGE fluid simulations including full $\boldsymbol{E}\times\boldsymbol{B}$ drifts. This larger extent provides opportunity for greater dissipation volume, but also further demonstrates that fully-2D simulations including cross-field drifts are required for detachment studies working towards a predictive capability of divertor heat loads.

1. INTRODUCTION

A future, high power density tokamak will rely on dissipation by radiation to distribute power around the full vessel surface before it can be concentrated on the divertor plate. In any tokamak of reasonable size, a hydrogen-fuelled plasma cannot, with hydrogen alone, radiate sufficiently to simultaneously dissipate enough of the input power and ensure that particle and heat fluxes to the target are below the damage threshold for any solid surface [1]. Dissipative processes, then, rely on impurities – any element of higher Z than the fuel – to radiate additional power through excitation, de-excitation, recombination, and spontaneous emission before it impinges on the wall, in particular in conditions consistent within the divertor volume; T_e of 1-100 eV and n_e of 10^{18}-10^{21}/m^3. Some intrinsic impurities may naturally erode by sputtering from the walls into the plasma due to plasma-wall interactions. If that is insufficient for dissipation by radiation, then additional extrinsic impurities injected by

puffing or some other means into the plasma will be required to provide the necessary radiative loss. However, this further increases the impurity concentration – i.e., the ratio of impurity density to the electron density, $c_z = n_z / n_e$, and too many impurities in the plasma can lead to core cooling and eventual dilution of the hydrogenic fuel and loss of fusion performance [2]. Thus, mechanisms to prevent these deleterious effects are under investigation including maintaining higher confinement with high toroidal field [3], and shielding the core from the divertor by controlling impurity leakage with closed divertor geometries [4], structures such as long-legged divertors [5], or gas box divertors [6].

At the same time, a number of parameterizations have been developed to quantify the impurity concentration required to adequately dissipate the extreme heat flux that will stream down the open field lines of a future fusion reactor. Based on simple scalings like that of Lengyel [7], these approaches suggest that the estimated extrinsic impurity concentrations required for detachment in ITER, FNSF, and DEMO can be >10% and thus detrimental for core dilution [8,9,10]. Other modelling efforts, however, have suggested that much lower concentrations may be sufficient for detachment of the outer leg in machines like FNSF [11] and ARIES-ACT [12]. While strongly conditional on machine projections for upstream conditions, power crossing the separatrix, energy and momentum losses, and radial size of a device, such modelling and scalings reveal that accurate measurements of impurity densities for a plasma in current devices are both rare and critical for their verification and validation. This is particularly true for measurements of c_z in the divertor region itself where impurities are 'diverted' away from the core, cool, and then are ultimately deposited on the wall or pumped away. In particular, questions such as mechanisms for dissipation, non-Coronal effects, the impact of E×B drifts and divertor asymmetries, the roles of intrinsic vs. extrinsic species, as well as that of transport and charge exchange processes, need to be answered to gain confidence in application to future devices.

2. PLASMA MEASUREMENTS

Spectroscopic measurements of emissions from plasma are used to measure the impurity content and determine the concentration of impurities species in the hydrogenic fuel. Two recent efforts for measurement of c_z under detached divertor conditions are those by Nakano, *et al*., for intrinsic C concentration in JT-60 [13,14], and that of Henderson, *et al*., for extrinsic N concentration required for detachment in JET and ASDEX-U [15,16]. Each relies on extensive spectroscopic diagnostics, both multi-chordal and 2-D imaging systems at visible or combined visible/VUV wavelengths, for both quantification of radiative impurity emissions and for inference of local plasma temperature and density from spectroscopic line ratios. In the current work, a unique method for measuring impurity densities, charge-state distributions, and concentrations in the plasma is presented which instead relies on direct measurement of plasma conditions in the divertor using Thomson scattering. This is accomplished thanks to the flexibility of an open divertor and the ability to leverage the radial coincidence of two key diagnostics: 1) spectroscopy measuring the line-integrated spectral radiance from all dominant fuel and impurity species emitting light in the divertor region, and 2) divertor Thomson scattering (DTS) [17], a system to measure electron temperature, T_e, and electron density, n_e, along the spectroscopic line of sight where the plasma radiates. For the latter, DTS offers fast sampling (10 ns) and repetition rate (50 Hz) with high measurement dynamic range ($0.5<T_e<200$ eV, $1E18<n_e<1E21/m^3$). A recent upgrade to the DIII-D DTS increased the number of sampling locations above the lower shelf of the open divertor from 8 to 12 channels, providing improved spatial distribution in key areas where the ionization front may lay under detached divertor scenarios (Fig. 2). Here, T_e and n_e are the controlling parameters determining rates for excitation, de-excitation, ionization, and recombination for each plasma species.

To extend 0 or 1-dimensional information about the divertor plasma to 2-D, the open nature of the lower divertor in DIII-D is used in conjunction with diagnostics that are inherently limited in spatial coverage, including 0-D line-integrated spectroscopy, and the 1-D DTS array (Fig. 1). In discharges with steady parameters (B_T, I_P, P_{inj}, $<n_e>$, core shaping/geometry), the OSP is positioned such that its conditions are sampled by the lowermost DTS chord and in direct view of the DivSPRED EUV/VUV spectrometer, with DTS chords at higher Z sampling the plasma at different ψ_n and L_{pol} (or L_{par}), and the DivSPRED integrating through the same vertical volume at a separate toroidal location. In order to gather information about other locations of the plasma, then, the divertor legs and X-point is swept [18], typically at

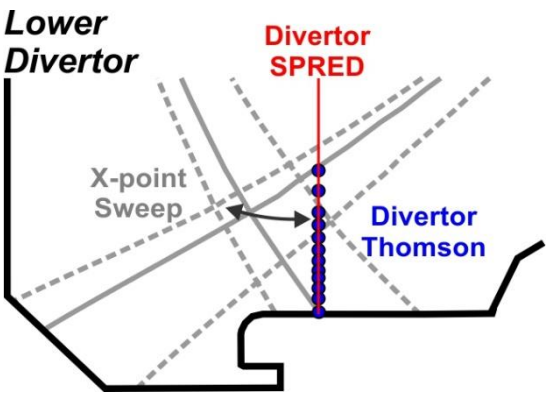

FIG 1. Sweeping of the divertor legs and X-point in relation to diagnostic coverage in the lower divertor of

a rate of 5-15 cm/s of plasma exposure to give adequate time to measure the plasma as it shifts position. Data from each sample period are mapped to the magnetic equilibria, and, when the sweep is complete, the data all collectively remapped to a single target equilibrium. Under the condition that plasma conditions along the divertor legs do not significantly change through the sweep [18], this allows a 2-D map of T_e, n_e, p_e data to be constructed from the DTS data (Fig. 2).

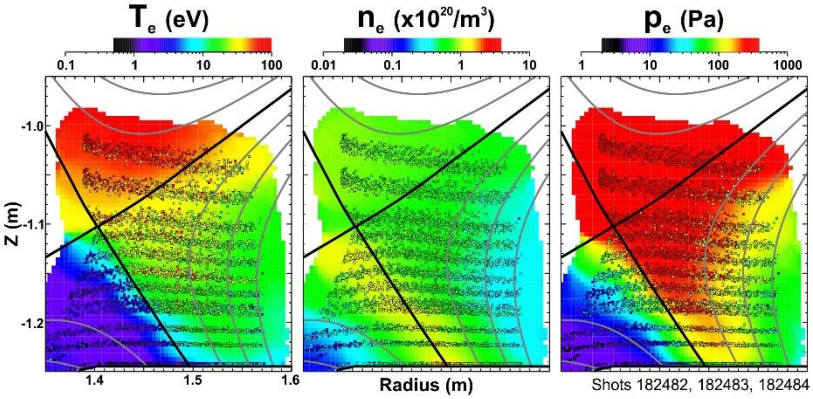

FIG 2. Inter-ELM electron conditions in the DIII-D divertor constructed using the expanded 12-channel lower shelf DTS diagnostic with points mapped to the equilibrium through a divertor sweep.

Knowledge of the plasma conditions spanning the line-integrated portion of the plasma where measured emissions originate uniquely allows those emissions to be interpreted. In the case of the work here, resonance emissions – i.e., those connected directly to the ground state – are utilized in order to avoid the need for consideration of metastable levels. For resonance emissions, the volume emission rate is expressed as $E_{ij}=Br_{ij}\cdot Q_{gnd\rightarrow p}\cdot n_i\cdot n_e$, [19] where the branching ratio, Br_{ij}, is equal to 1, and the electron impact excitation rate from the ground to the p state, $Q_{gnd\rightarrow p}$, is dependent only on T_e and n_e. For low and medium-Z elements, however, resonance emissions are primarily in the EUV/VUV spectral region, necessitating a spectrometer that is directly vacuum connected on the machine. On DIII-D, this spectrometer, the divertor SPRED (DivSPRED) is a Survey, Poor Resolution, Extended Domain grazing-incidence instrument [20,21]. With a low density 290 gr/mm grating allowing the observed bandwidth to span the 25-165 nm region, the spectrometer was originally calibrated for absolute intensity sensitivity at the NIST SURF facility [22], and that calibration modified for a new viewing geometry and camera using the branching ratio technique associating the intensity of EUV lines to those in other emission bands which are more directly calibrated [23]. Due to their typically high intensity, the system is capable of regular spectral line measurements at >500 Hz operation. A sample for standard emissions for the carbon impurity background in DIII-D are shown in Fig. 3, each line fit with a 1.0 nm wide Gaussian profile representative of the instrumental width of the spectrometer. It is notable that the observed bandwidth also contains a similar capability for multiple impurity species monitoring for extrinsic impurities like N, Ne, and Ar.

3. CHARGE-STATE AND SPECTRAL SYNTHESIS

If conditions in the plasma are known with sufficient spatial resolution, then the plasma may be modelled given rate equations for populating mechanisms and level populations for the neutrals and ions. Processes that may occur in the plasma include excitation, de-excitation, electron impact ionization, recombination, and spontaneous emission. If rates for all transitions are known, then a generalized collisional radiative (GCR) model may be developed and applied to describe all the possible ways for a process to occur, and thus determine the steady state equilibrium ground and excited state populations for each impurity species being modelled for given plasma conditions. This is accomplished in the recently-developed ColRayPy python-based code described in [24], using ADF04 resolved specific ion process rates from the ADAS database [25]. Further, the code also is able to calculate photon emissivity coefficients (PEC) – the population of a level multiplied by its spontaneous emission coefficient, which allow the determination of spectral line intensities for all known transitions. In an ionized

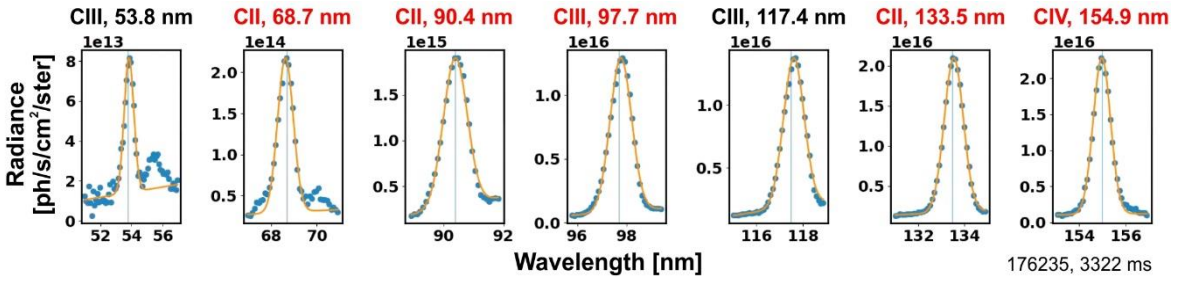

FIG 3. EUV/VUV line emissions for carbon fit with 5-parameter Gaussian functions. Resonance emissions are labeled in red.

plasma, the emission of any spectral line for the transition from level i to *j*, $\epsilon_{i\to j}$, is then the contribution of PECs for each of excitation (exc), recombination (rec), and charge exchange (CX), as follows:

$$\epsilon_{i\to j} = \sum_\sigma PEC^{(exc)}_{\sigma,i\to j} n_e n_\sigma^{z+} + \sum_\rho PEC^{(rec)}_{\rho,i\to j} n_e n_\sigma^{(z+1)+} + \sum_\rho PEC^{(CX)}_{\rho,i\to j} n_D n_\sigma^{(z+1)+} \text{ (ph/s/cm}^3\text{)} \qquad \text{Eqn. 1}$$

with dependencies of both impurity and electron densities, and in the case of CX, the neutral density. Using this approach, collisional radiative modelling with metastable transition state treatment is applied to two problems shown in Fig. 4: a) A constant density plasma with increasing temperature to determine how the population fraction or relative abundancy evolves, and b) synthesize all of the emissions a plasma at a given temperature and density will produce in order to identify which species and therefore which transitions are necessary to accurately model the plasma. Both are carried out for carbon, the dominant intrinsic impurity in DIII-D. The plot of PEC vs. wavelength demonstrates how the brightest radiant emissions are found in the region of 0-200 nm – the deep UV and EUV/VUV – and that spectral emissions for higher charge states are typically found at shorter (more

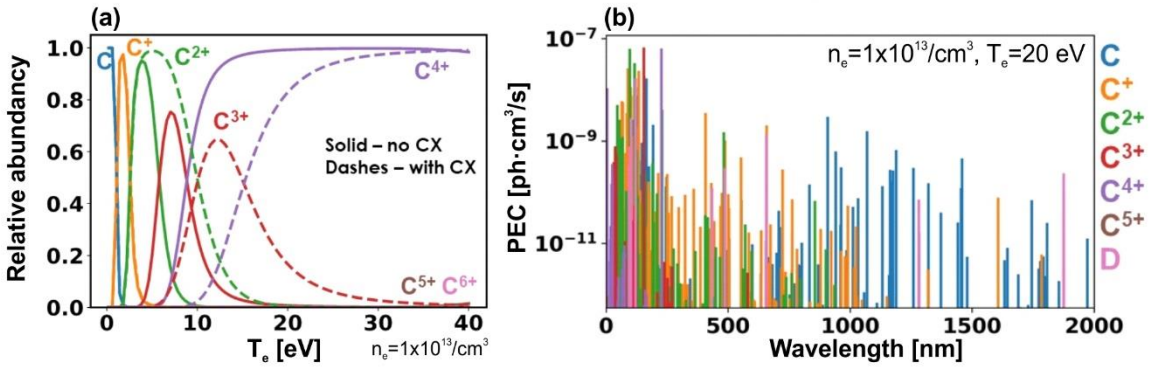

FIG 4. a) Charge state distribution for carbon under constant density conditions, showing the impact of CX. b) Photon emissivity coefficients for all C and D lines in the ADAS database for constant T_e, and n_e in the range of 0-2 μm.

energetic) wavelengths. In the plot of relative abundancy vs. T_e, cases both with and without charge exchange are evaluated, demonstrating how much impact such contribution may have. In the case shown, the neutral density is taken as a fraction of the n_e, parameterized vs. T_e as determined from UEDGE, and the neutral Deuterium atom temperature, T_D, is set to be equal to ϵ_{FC}=3.5 eV, which is representative of a Franck-Condon contribution in the D_2 molecular breakup process [26,27].

4. IMPURITY CONCENTRATION WORKFLOW

With the capability to both measure local plasma parameters, and to synthesize the equilibrium population distribution and spectral profile for known transition lines with ColRadPy, a more complete analysis of the divertor can be approached. Employing a measured and synthetic result, the primary dependent variable is the ratio of n_z/n_e in Equation 1, thus the impurity concentration may be determined based on matching the measurement to the synthetic spectra. The workflow for this work is shown in Fig. 5, where the measured spectra is compared to a synthetic spectrum created using DTS and a neutral density and estimates for transport parameters from modelling codes like UEDGE. In a tokamak divertor, plasma conditions can vary significantly on spatial scales of ~1 cm. For 1D radial emission profiles, the finite radial width of the DTS measurement (~3 mm) and the DivSPRED cone (~40 mm) are accounted for by smoothing of the result over the appropriate spatial scale to compare directly to an

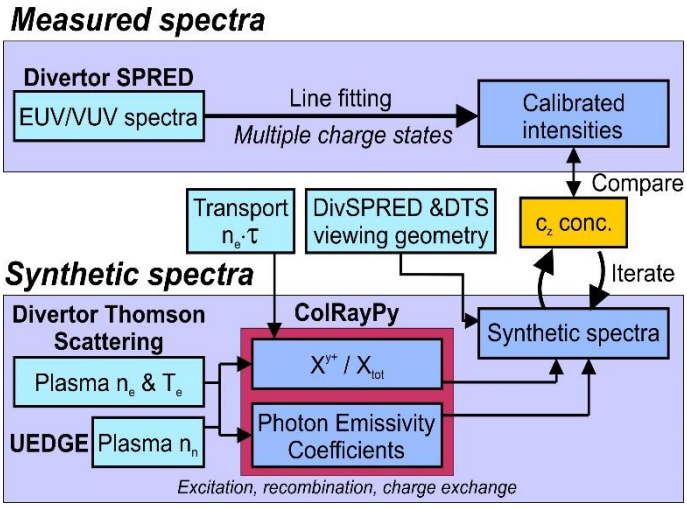

FIG 5. Workflow for iteratively solving for the impurity concentration in the plasma.

experimentally measured result. This value may be iterated in the synthetic spectra calculation. In the case of the divertor, however, the line-integrated emission in the vertical view of the DivSPRED spectrometer (Fig. 1) is split into the summation of many discrete piecewise components representative of the local plasma measurement by the DTS array. Once the total of those components are summed to a calibrated spectrum which compares well with the experimental spectrum, the c_z is found.

This match, however, requires a metric on the match to all emission lines simultaneously – e.g., weighting the most prominent emission lines where dynamic range is the highest, lines in the part of the spectrum where the calibration is known with the greatest confidence, or lines where atomic rates and PECs are known to be the most accurate. The capability to simplify the synthetic solution to include only the most basic process of excitation, or remove and/or modify physical processes like charge exchange, or transport in the n_e parameter, and re-run a case quickly (<10 minutes of processing time) makes this approach a very flexible mechanism to explore the dominant processes at play in the divertor employing this workflow.

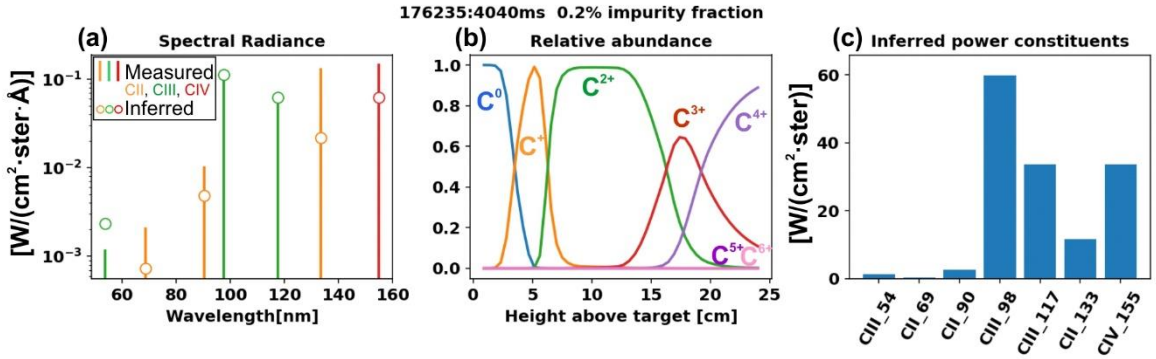

FIG 6. Results from detached plasma case where n_C/n_e is inferred to be 0.2%, showing a) spectral radiance from all target emissions where lines are the measured data and circles are the experimentally inferred result, b) the relative abundance of each C charge state vs. height above the lower shelf, and c) line-integrated radiated power from each emission constituent.

5. RESULTS

A test case is chosen with parameters of P_{inj}=4.5MW, B_T=2.05T, I_p=1.25MA, with ion B×∇B drift towards the primary X-point in DIII-D's 'shelf' open divertor, a DIII-D discharge that has been previously modelled [28,29]. This plasma discharge includes a density ramp such that the divertor transitions from being a well attached target ($T_{e,t}$~20 eV) to detached ($T_{e,t}$~1 eV). In this shot, the only primary radiator is the intrinsically eroded carbon from the graphite walls of DIII-D; only this is considered here to assess the capabilities of the measurement/code workflow, and avoid the complication of multiple radiating impurities. Charge exchange is included in the synthetic model, where in the absence of a neutral density measurement, n_D is based on a parameterization taken from UEDGE for the full grid. Fig. 6 shows results in the detached phase of this shot. Using the workflow described, the inter-ELM intrinsic carbon impurity fraction in DIII-D was found to be 2-5% in attached H-mode conditions, falling to ≤0.5% in detached conditions while maintaining about the same total absolute carbon density. UEDGE modelling with a full physics drift model [30] similarly shows a reduction in impurity concentration in detachment but limited to a 2.8× drop.

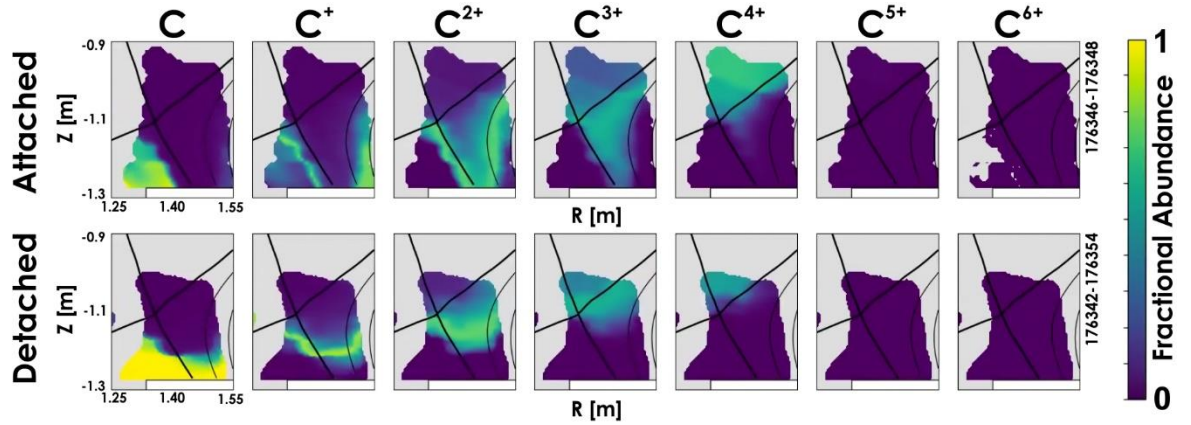

FIG 7. Inferred 2D spatial distribution of charge states in attached (top row) and detached (bottom row) DIII-D plasmas.

Using the same set of calibrated EUV/VUV spectroscopy and DTS T_e and n_e measurements, now in a full 2-D geometry, the workflow can be applied to a full map in radial and Z space in the machine, producing the fractional abundance for each charge state. Fig. 7 shows these charge state distributions for a the well attached case ($T_{e,t}$~20 eV) on top where the carbon population is inferred to be dominated by C^{2+} in the divertor, and the detached plasma condition ($T_{e,t}$~1 eV) on the bottom row. In contrast to the attached phase, the detached plasma shows highly radiating narrow bands of C^{+} and C^{2+} at the detachment front. In both cases, C provides >50% of the total radiation in the divertor from emission by CII, CIII, and CIV [21].

6. COMPARISON TO UEDGE

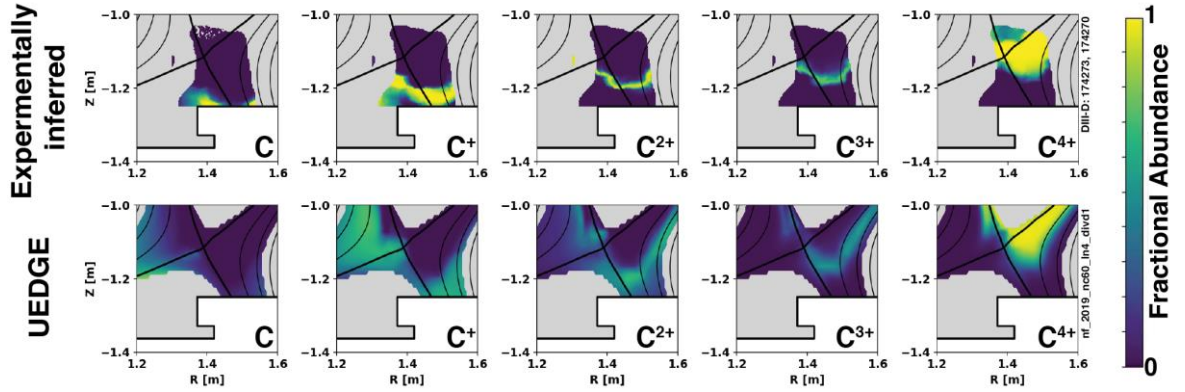

FIG 8.Comparison of relative carbon impurity charge states in a detached open divertor showing similar charge-state composition throughout the detachment front in both experimentally inferred and simulated abundancies.

The charge state distribution comparison with UEDGE modelling displays quantitatively similar 2D profiles to those experimentally inferred albeit with an additional charge-state mixing caused by the finite lifetime of ions as they are transported via parallel flows that are not accounted for in the collisional radiative model (Fig. 8). For the experimentally inferred case, however, charge exchange is not included, which leads to significantly more stratification of the charge states in the 2D profiles inferred from the DTS and DivSPRED data (top row) compared to the lower row of Fig. 7. This suggests that charge exchange is indeed an important process at play in the detached divertor.

The radial extent of the radiative volume in detached H-mode discharges has also been shown to display broader features in detached H-mode discharges compared to UEDGE fluid modelling (5.2MW, 0.9MA, 1.8T, $\boldsymbol{B} \times \nabla B$ drift towards the primary X-point) [31] with an increasing level of broadening observed at higher powers [32]. This broad feature in the carbon profile in particular is observed in both charge-state resolved line emission (Fig. 9). UEDGE simulations with drifts and currents with comparisons to total radiated power (bolometry), Divertor Thomson Scatting, and 2-D visible imaging show that in these conditions the poloidal $\boldsymbol{E} \times \boldsymbol{B}$ drift can dominate the poloidal heat transport in the radiative front, expanding the poloidal extent of the radiation front as well as increasing the total radiative power [29]. This indicates a larger volume for dissipation may be achievable in future devices, and an enhanced ability for divertor radiation to be the principal mechanism by which power is exhausted in the SOL compared to the more commonly used 1-D and 0-D modelling approximations, or 2-D modelling without drifts. This directly impacts our ability to predict detachment onset, detachment

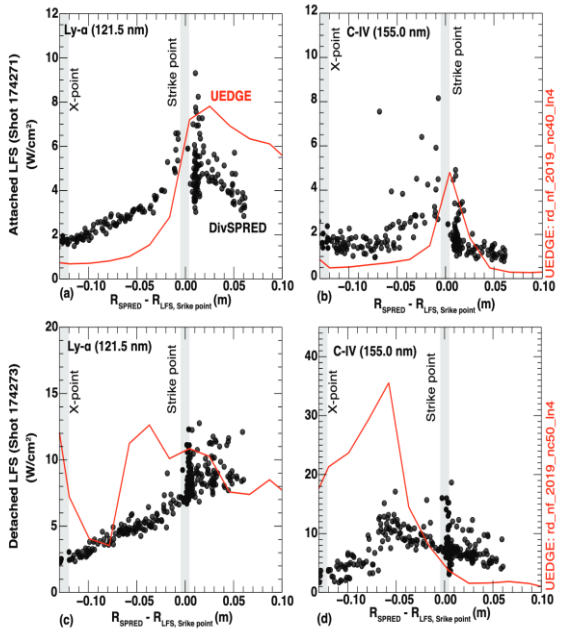

FIG 9. Comparison of constituent species emission in the EUV/EUV (dots) with UEDGE fluid simulations (lines) in medium density attached (top) and detached (bottom) conditions showing acceptable agreement in attached conditions (top) but overpredictions in emission height while underpredicting radial emission extent in detached conditions. Figure from [4]

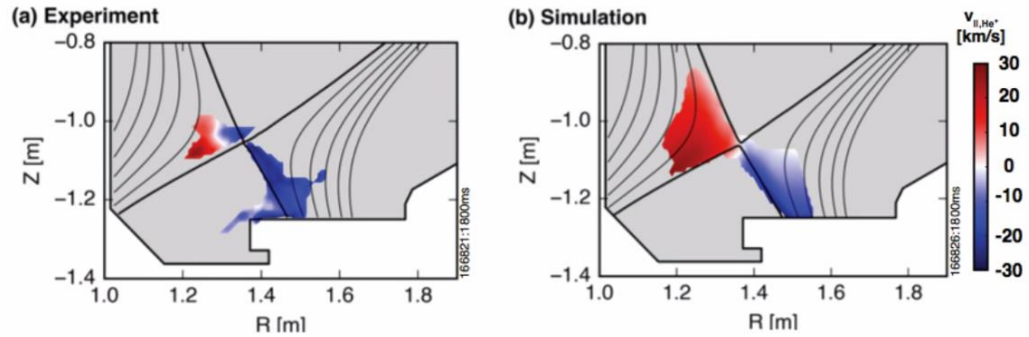

FIG 10. He^+ flow velocity measured by the DIII-D CIS diagnostic, and b) flow modeled with UEDGE.

stability, the impurity fraction required to achieve detachment, and the heat flux mitigation that can be expected in planned divertors

Finally, quantitative 2D comparison between UEDGE-predicted and measured flows has recently been achieved using velocity imaging (Fig. 10) [33]. Using Doppler coherence for 2D ion velocity measurements [34], agreement of He^+ velocities in a pure helium L-mode plasma is achieved near the divertor target where He is the main-ion species and electron physics dominates. Further upstream where ion-dominated physics plays a more important role, a factor of 2–3 underestimation of the velocity is observed. This result indicates an underestimation of the role of ions in determining local plasma characteristics near the X-point that impacts our ability to predict impurity transport via parallel flows in the divertor, estimate convective power fraction in detached conditions, and establish total pressure dissipation.

7. CONCLUSIONS AND FUTURE WORK

Leveraging the key combination of coincident plasma parameter and emission characterization on DIII-D, combined with a generalized collisional radiative model makes it possible to rapidly determine the charge-state distribution and impurity concentration in the plasma, elucidate the physics underlying detachment processes in the divertor and reveal the 2D nature of detachment important for design of detachment scenarios for next stage devices. The workflow described here employs reduced models which are useful for informing how time-consuming modelling with large models with electromagnetic drifts are run, as a useful step in the hierarchy of increasing simulation sophistication. These measurements and their comparison to boundary modelling are critically essential for validation of recent scalings for the impurity concentration required for detachment in future fusion devices. Direct quantitative comparison to modelling demonstrates a greater radial emission extent compared to UEDGE fluid simulations, possibly allowing for greater than expected dissipation volume.

Future work will expand the database of discharges explored with the model described, and include cases with extrinsic impurity injection of N, Ne, and Ar, all of which display emissions from multiple charge states in the observed bandwidth of the DivSPRED diagnostic. Incorporation of an additional diagnostic – the 2-D tangential visible imagining system – will allow for an additional experimental comparison to the results derived here, and make direct validation of the approach for impurity concentration measurement employed at JET/ASDEX-U possible.

ACKNOWLEDGEMENTS

This material is based upon work supported by the U.S. Department of Energy, Office of Science, Office of Fusion Energy Sciences, using the DIII-D National Fusion Facility, a DOE Office of Science user facility, under Award(s) DE-FC02-04ER54698, DE-AC52-07NA27344, DE-NA0003525, and DE-SC0015877. **Disclaimer**: This report was prepared as an account of work sponsored by an agency of the United States Government. Neither the United States Government nor any agency thereof, nor any of their employees, makes any warranty, express or implied, or assumes any legal liability or responsibility for the accuracy, completeness, or usefulness of any information, apparatus, product, or process disclosed, or represents that its use would not infringe privately owned rights. Reference herein to any specific commercial product, process, or service by trade name, trademark, manufacturer, or otherwise does not necessarily constitute or imply its endorsement, recommendation, or favoring by the United States Government or any agency thereof. The views and opinions of authors expressed herein do not necessarily state or reflect those of the United States Government or any agency thereof.

REFERENCES

[1] LOARTE, A., MONK, R.D., MARTIN-SOLIS, J.R., *et al*., "Plasma detachment in JET Mark I divertor experiments", Nucl. Fusion **38** (1998) 331.

[2] DUX, R., PEETERS, A.G., "Neoclassical impurity transport in the core of an ignited tokamak plasma", Nucl. Fusion **40** (2000) 1721.

[3] KUANG, A.Q.,BALLINGER, S., BRUNNER, D., *et al.*, "Divertor heat flux challenge and mitigation in SPARC", J. Plasma Physics **86** (2020) 1.

[4] CASALI, L., ELDON, D., BOEDO, J.A., *et al*., "Neutral leakage, power dissipation, and pedestal fuelling in open vs. closed divertors", Nucl. Fusion **60** (2020) 076011.

[5] UMANSKY, M.V., LABOMBARD, B., BRUNNER, B., *et al*., "Attainment of a stable, fully detached plasma state in innovative divertor configurations", Phys. Plasmas **24** (2017) 056112.

[6] GOLDSTON, R.J., MYERS, R., SCHWARTZ, J., "The lithium vapor box divertor", Physica Scripta **T167** (2016) 014017

[7] LENGYEL, L.L., "Analysis of radiating plasma boundary layers", IPP Report I (1981) 191.

[8] GOLDSTON, R.J., REINKE, M.L., SCHWARTZ, J.A., "A new scaling for divertor detachment", Plasma Phys. Control. Fusion **59** (2017) 055015.

[9] REINKE, M.L., "Heat flux mitigation by impurity seeding in high-field tokamaks", Nucl. Fusion **57** (2017) 034004.

[10] KALLENBACH, A., BERNERT, M., DUX, R., *et al*., "Analytical calculations for impurity seeded partially detached divertor conditions", Plasma Phys. Control. Fusion **58** (2016) 045013.

[11] ROGNLIEN, T.D., RENSINK, M.E., STOTLER, D.P., "Scrape-off layer plasma and neutral characteristics and their interactions with walls for FNSF", Fusion Eng. and Design **135** (2018) 380.

[12] RENSINK, M.E., ROGNLIEN, T.D., "Plasma heat-flux dispersal for ACT1 divertor configurations", Fusion Sci. and Tech. **67** (2014) 125.

[13] NAKANO, T., KUBO, H., ASAKURA, N., *et al*., "Volume recombination of C^{4+} in detached divertor plasmas of JT-60U", Nucl. Fusion **47** (2007) 1458.

[14] NAKANO, T., KUBO, H., ASAKURA, N., *et al*., "Radiation process of carbon ions in JT-60U detached divertor plasmas", J. Nucl. Materials **390-391** (2009) 255.

[15] HENDERSON, S., BERNERT, M., BREZINSEK, S., *et al*., "Determination of volumetric plasma parameters from spectroscopic N II and NIII line ratio measurements in the ASDEX Upgrade divertor", Nucl. Fusion **58** (2018) 016047.

[16] HENDERSON, S., BERNERT, M., BREZINSEK, S., *et al*., "An assessment of nitrogen concentrations from spectroscopic measurements in the JET and ASDEX upgrade divertor", Nucl. Mat. And Energy **18** (2019) 147.

[17] GLASS, F., CARLSTROM, T.N, Du, D., *et al*., "Upgraded divertor Thomson scattering system on DIII-D", Rev. Sci. Instrum. **87** (2016) 11E508.

[18] MCLEAN, A.G., LEONARD, A.W., MAKOWSKI, M.A., *et al*., "Electron pressure balance in the SOL through the transition to detachment", J. Nucl. Mater. **463** (2015) 533.

[19] TERRY, J.L., CHEN, K.I, MOOS, H.W., *et al*., "EUV impurity study of the Alcator tokamak", Nucl. Fusion **18** (1978) 485.

[20] FONCK, R.J., RAMSEY, A.T., YELLE, R.V., "Multichannel grazing-incidence spectrometer for plasma impurity diagnosis: SPRED", Applied Optics **21** (1982) 2115.

[21] MCLEAN, A.G., JAERVINEN, A., BRIESEMEISTER, A., *et al.*, "Quantification of radiating species in the DIII-D divertor in the transition to detachment using extreme ultraviolet spectroscopy", 2018 IAEA FEC 2018 EC/PC-15.

[22] WOOD, R.D., ALLEN, S.L., "Absolute calibration of a SPRED EUV spectrograph for use on the DIII-D tokamak", Rev. Sci. Instrum. **59** (1988) 1537.

[23] DALTRINI, A.M., MACHIDA, M., "Modified branching ratio method for absolute intensity calibration in VUV spectroscopy", IEEE Trans. On Plasma Science **33** (2005) 1961.

[24] JOHSON, C.A., LOCK, S.D., ENNIS, D.A., "ColRadPy: A Python collisional radiative solver", Nuclear Materials and Energy **20** (2019) 100579.

[25] SUMMERS, H.P. (2004) The ADAS User Manual, version 2.6 http://www.adas.ac.uk

[26] NAKAMURA, M., TOGO, S., ITO, M., *et al*., "One-dimensional time dependent analysis of the detachment front in a divertor plasma: Roles of the cross-field transport", Plasma and Fusion Res. **6** (2011) 2403098.

[27] JANEY, R.K., *et al*., (1987) Elementary Processes in Hydrogen-Helium Plasmas (Berlin: Springer)

[28] ROGNLIEN, T.D., MCLEAN, A.G., FENSTERMACHER, M.E., *et al*., "Comparison of 2D simulations of detached plasmas with divertor Thomson measurements in the DIII-D tokamak", Nucl. Mater. And Energy **12** (2017) 44.

[29] JAERVINEN, A.E., ALLEN, S.L., ELDON, D., *et al*., "$\boldsymbol{E \times B}$ flux driven detachment bifurcation in the DIII-D tokamak", Phys. Rev. Letters **121** (2018) 075001.

[30] JAERVINEN, A.E., ALLEN, S.L., LEONARD, A.W., *et al*., "Role of poloidal $\boldsymbol{E \times B}$ drift in divertor heat transport in DIII-D", Contrib. Plasma Phys **10** (2019) 1002.

[31] JAERVINEN, A.E., ALLEN, S.L., ELDON, D., *et al*., "Progress in DIII-D towards validating divertor power exhaust predictions", Nucl. Fusion **60** (2020) 056021.

[32] LEONARD, A.W., JAERVINEN, A.E., MCLEAN, A.G., *et al*, "MHD stability constraints on divertor heat flux width in DIII-D", IAEA 2020 (this meeting).

[33] SAMUELL, C.M., PORTER, G.D., MEYER, W.H., *et al*., "2D imaging of helium ion velocity in the DIII-D divertor", Phys. Plasmas **25** (2018) 056110.

[34] SAMUELL, C.M., PORTER, G.D., MEYER, W.H., *et al*., "Verification of Doppler coherence imaging for 2D ion velocity measurements on DIII-D", Rev. Sci. Instrum. **89** (2018) 093502.